Inorganic Chemistry

Article

pubs.acs.org/IC

Perovskite to Postperovskite Transition in $NaFeF_3$

Fabian L. Bernal,[†] Kirill V. Yusenko,[†] Jonas Sottmann,[†] Christina Drathen,[‡] Jérémy Guignard,[‡] Ole Martin Løvvik,[§] Wilson A. Crichton,[‡] and Serena Margadonna*[,†]

[†]Chemistry Department and Centre for Material Science and Nanotechnology and [§]Department of Physics, University of Oslo, NO-0315 Oslo, Norway

[‡]ESRF—The European Synchrotron, 71, Avenue des Martyrs, Grenoble 38043, France

Supporting Information

ABSTRACT: The $GdFeO_3$-type perovskite $NaFeF_3$ transforms to $CaIrO_3$-type postperovskite at pressures as low as 9 GPa at room temperature. The details of such a transition were investigated by in situ synchrotron powder diffraction in a multianvil press. Fit of the $p-V$ data showed that the perovskite phase is more compressible than related chemistries with a strongly anisotropic response of the lattice metrics to increasing pressure. The reduction in volume is accommodated by a rapid increase of the octahedral tilting angle, which reaches a critical value of 26° at the transition boundary. The postperovskite form, which is fully recoverable at ambient conditions, shows a regular geometry of the edge-sharing octahedra and its structural properties are comparable to those found in $CaIrO_3$-type $MgSiO_3$ at high pressure and temperature. Theoretical studies using density functional theory at the GGA + U level were also performed and describe a scenario where both perovskite and postperovskite phases can be considered Mott–Hubbard insulators with collinear magnetic G- and C-type antiferromagnetic structures, respectively. Magnetic measurements are in line with the theoretical predictions with both forms showing the typical behavior of canted antiferromagnets.

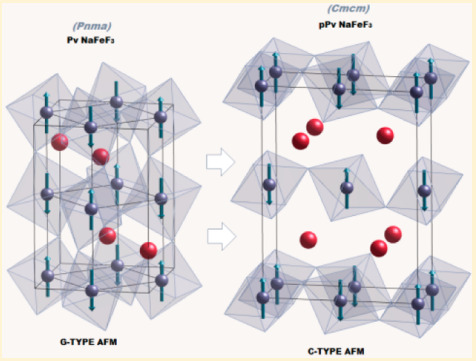

INTRODUCTION

Transition metal fluorides with the general formula $AM^{2+}F_3$ have been intensively studied in the past as the versatile spatial arrangement of the MF_6 octahedra can support a variety of electronic, magnetic, and structural behaviors.[1] For instance, the $KM^{2+}F_3$ (M^{2+} = Mn, Fe, Co, Ni) systems that have been studied since the early 1960s adopt perovskite-type structures and order antiferromagnetically with Néel temperatures T_N as high as 280 K.[2] The pseudocubic perovskite $KCuF_3$ behaves as an orbitally ordered one-dimensional S = 1/2 Heisenberg antiferromagnet,[3] while $KCrF_3$, which also adopts the $KCuF_3$($tI20$)-type structure, displays a very complicated scenario of interplay between the lattice, orbital, and spin degrees of freedom reminiscent of the behavior of the CMR manganites.[4] Furthermore, transition metal fluorides with the tetragonal tungsten bronze structure (e.g., $K_{0.6}FeF_3$) have been identified as key systems to display multiferroism where particular charge ordering patterns induce ferroelectricity.[5]

In addition to these, the $GdFeO_3$-type $NaM^{2+}F_3$ fluorides (M = Ni, Co, Mg, Mn, and Zn) are also receiving attention as they are considered to be among the best analogous compounds to study the perovskite to postperovskite ($CaIrO_3$-type) transition occurring in $MgSiO_3$ in the D″ region of the mantle.[6−9] Much theoretical and experimental work has been devoted to this transition given its importance for the understanding of the structure of the deep Earth.[10−12] However, further advances are impeded by the extreme conditions of temperature and pressure that are needed to reproduce the actual conditions at the D″ layer (125 GPa and 2500 K) and beyond. For this reason studies of the behavior of related systems that also undergo perovskite (Pv) to postperovskite (pPv) transitions, but at more easily accessible conditions, have been undertaken opening the way to an improved understanding of the implication that such a transition might have on different phenomena (e.g., seismic anisotropy) occurring at the core–mantle boundary.[12] In the fluorides, the Pv to $CaIrO_3$-type pPv phase transition occurs at conditions that are readily available to multianvil presses (e.g., 10–20 GPa and 800–1473 K). In the case of $NaNiF_3$, the pPv phase forms at 16–18 GPa and 1273–1473 K and is fully recoverable at ambient conditions.[8,9] While both $NaCoF_3$ and $NaZnF_3$ transform at similar conditions, the pPv phase is only partially quenchable upon decompression at room temperature.[6−9,12−15] In all cases, the Pv–pPv transition is accompanied by relatively small volume changes (1–2%) and the Clapeyron slopes of the boundaries have large positive values (10 and 17 MPa/°C) which are directly comparable to that found in $MgSiO_3$.[14] Very importantly, in the fluorides, the Pv to pPv transition can also be observed at room temperature using diamond anvil cells (DACs) and it occurs at 28–30 GPa in $NaMgF_3$, while lower pressures, in the range between 11 and 14 GPa, are needed for M = Ni, Co, and Zn.[8,9,13] Further laser

Received: September 12, 2014
Published: October 29, 2014

heating in DACs of the so-formed pPv phases induces a transition to a yet unknown structure in $NaMgF_3$ (a so far elusive possible post-pPv phase),[7] to decomposition to CsCl-type NaF + MgF_2, and to more complex disproportionation in $NaCoF_3$.[8] Up to now, accurate structural refinement of pPv fluoride phases has been achieved only for $NaNiF_3$.[9]

$NaFeF_3$ is another member of the fluoroperovskite family and is attracting interest as an efficient and stable cathode material for secondary Na ion batteries. Very surprisingly, little is currently known on the structural and magnetic properties of $NaFeF_3$ as a function of temperature and pressure. At ambient conditions, it adopts the $GdFeO_3$-type structure which was determined by single-crystal methods by Benner and Hoppe.[16] Careful inspection of the reported lattice parameters and atomic coordinates quickly identify that $NaFeF_3$ possesses all the important prerequisites (values of tolerance factor, tilting angle, and polyhedral volume ratio) to undergo a transition to a $CaIrO_3$-type phase at very amenable conditions. Indeed, we were recently successful in observing the Pv−pPv transition between 10 and 12 GPa in single-crystal samples of $NaFeF_3$, which were hydrostatically compressed using DACs at room temperature.[17] Very interestingly, further increase in pressure up to 20 GPa results in the stabilization of a post-postperovskite Sb_2S_3-type structure. This is the first experimental observation of any higher pressure forms beyond $CaIrO_3$ type in any system and is calculated as a stable enthalpy-driven form only for Al_2O_3 (at 3.6 Mbar),[18] while it is calculated as metastable in $NaMgF_3$.[19] The equivalent pressure, for $MgSiO_3$, is estimated at 1.6 TPa, though this is also estimated to be metastable.[20] The understanding of such a transition allows for the construction of a unified framework where possible structural sequences in perovskites and the competitive sesquioxides can be predicted beyond pPv, over a much wider range of chemistries. The realization that $NaFeF_3$ undergoes the transformation to pPv at lower pressures (in single-crystal specimens at room temperature (RT)) than other members of the family has prompted us to further investigations with the aim of defining a general description of the Pv−pPv transition in fluoroperovskites to compare and contrast with those proposed for the ABO_3 analogues.

Here we report on the synthesis of polycrystalline pPv $NaFeF_3$ using multianvil apparatus together with a detailed description of the structural and magnetic properties of both Pv and pPv forms of $NaFeF_3$. The results of synchrotron powder X-ray diffraction measurements, magnetometry, and ab initio density functional theory (DFT) calculation will be discussed.

EXPERIMENTAL SECTION

Polycrystalline samples of Pv $NaFeF_3$ samples were synthesized according to ref 16. Degassed NaF, Fe, and FeF_3 powders were finely ground and mixed in a 3:2:1 ratio. The so-obtained mixtures were then pelletized and loaded into an Fe tube which was used as a reaction vessel. All the manipulations were carried out in an Ar-filled glovebox, given the hygroscopic nature of NaF, and to avoid exposure to oxygen and/or moisture. The Fe tube was tightly closed and then heated under a constant nitrogen flow at 750 °C for 8 days.

The cubic multianvil press available at ID06LVP at the ESRF was used for the synthesis of pPv $NaFeF_3$. A 2 mg sample of the original Pv phase was packed into an hBN (Goodfellow) capsule, before being included into the 10/4 windowed Cr:MgO assembly (Ceramic Substrates). Pressure was generated using the 2000 ton MAVO press in 6/8(×32) mode, with carbide anvils. Pressures were estimated using the equation of state of BN, and a graphite furnace was used to achieve high temperatures. Synchrotron powder diffraction data were collected during all the steps of the synthesis and were recorded using a linear pixelated GOS detector from Detection Technology, running 32 sequential exposures at 10 Hz at 32 s intervals and mounted to intercept the downstream diffraction from the horizontal anvil gap at a distance of ∼1180 mm from the sample. The detector, beam-normal plane was mechanically corrected for tilt and rotation and the detector position and zero offset was calibrated against SRM660a, at a monochromatic wavelength of 0.3757 or 0.2254 Å, selected from the emission of a U18 undulator (6.1−6.2 mm gap) by a Cinel Si(111) double-crystal monochromator. Selected data for refinement were also collected using a Tl:NaI scintillator counter, with a 0.2 mm pinhole and receiving slits at intermediate distance, which acted as collimators of background scattering coming from the cell assembly. In this case, the effective radius of the pseudorotation detector arm was 1350 mm. Collimated beam sizes were 0.5 mm horizontal by 1 mm, or the vertical anvil gap, when smaller.

Ambient pressure high-resolution synchrotron X-ray diffraction experiments were performed on beamline ID31 at the ESRF. Finely ground samples of both Pv and recovered pPv $NaFeF_3$ were sealed in 0.5 mm diameter thin-wall glass capillaries. Diffraction profiles were recorded at various temperatures in the range T = 10−300 K (λ = 0.399 92 Å). The data were binned in the 2θ range 0.1−30° to a step of 0.002°. All the powder diffraction profiles collected at ID06 and ID31 were analyzed using the GSAS suite of Rietveld programs.[21,22]

The dc magnetization measurements of Pv and pPv $NaFeF_3$ were performed on a Quantum Design PPMS system and on a Quantum Design MPMS magnetometer, respectively. The temperature dependence of magnetization was determined following zero-field-cooled and field-cooled (ZFC, FC) protocols in magnetic fields H = 0.01, 0.1, and 1 T. Magnetic hysteresis loops up to H = 9 T for Pv and H = 5 T for pPv were collected at various temperatures.

Electronic structure calculations were performed with the Vienna ab initio simulation package (VASP)[23,24] using the PBE generalized gradient approximation (GGA).[25] The cutoff energy of the plane wave basis set expansion was 500 eV, and the density of the k-points was determined by a maximum distance of 0.25 $Å^{-1}$. All structures were relaxed with remaining forces lower than 0.05 eV/Å, using a quasi-Newton method.

RESULTS

Perovskite $NaFeF_3$: Crystal Structure and Magnetic Properties. Inspection of the high-resolution synchrotron powder diffraction profile at room temperature readily confirms the synthesis of a single-phase polycrystalline sample of $NaFeF_3$, adopting the orthorhombic $GdFeO_3$-type structure ($a = c \sim \sqrt{2}a_p$, $b \sim 2a_p$, where a_p is the lattice constant of the pseudocubic perovskite cell). Analysis by the Le Bail pattern decomposition technique resulted in lattice parameters a = 5.66119(2) Å, b = 7.88006(2) Å, and c = 5.48359(4) Å (space group *Pnma*), in agreement with previous work.[16] The final Rietveld refinement shows that the structure can be described as a three-dimensional network of almost regular corner-sharing FeF_6 octahedra (Figure 1).

The values of the metal−fluorine distances are consistent with the presence of the weakly Jahn−Teller distorted Fe^{2+} ions in high-spin (HS) electronic configuration and can be divided into medium bonds (2.072(1) Å) along the b-axis and alternating longer (2.085(1) Å) and shorter (2.052(1) Å) bonds in the ac plane, resulting in a very small value of the octahedral distortion parameter, $\Delta d = 42.2 \times 10^{-6}$. The orthorhombic distortion is then purely driven by the relative sizes of the ions as indicated by the calculated tolerance factor, t = 0.85. It is well-known that the value of $t \sim 0.9$ is considered the lower boundary for the stabilization of cubic perovskites. The small size of the 8-fold coordinated Na^+ cation induces tilting of the octahedra and distortion from the ideal cubic Pv

dx.doi.org/10.1021/ic502224y | Inorg. Chem. 2014, 53, 12205−12214

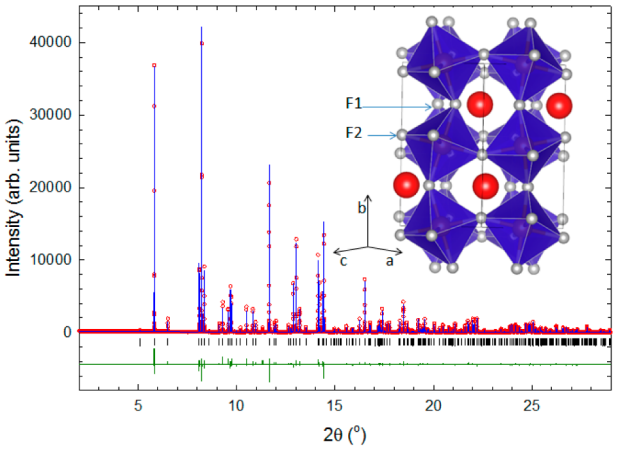

Figure 1. Final observed (○) and calculated (|) synchrotron X-ray diffraction profiles (λ = 0.3999 Å) for Pv $NaFeF_3$ at 298 K (a = 5.66119(2) Å, b = 7.88006(2) Å, and c = 5.48359(4) Å, space group *Pnma*). Agreement factors of the Rietveld refinement: R_{wp} = 8.07%; R_{exp} = 5.20%. The lower solid line is the difference profile, and the tick marks show the reflection positions. Small impurity peaks corresponding to α-Fe are also present in the diffraction profile (weighted phase fraction < 0.5%).

structure. The tilt angle ϕ, which represents the rotation of the FeF_6 octahedra about the pseudocubic [111] axis, can be calculated directly from the orthorhombic lattice constants ($\phi = \cos^{-1}(\sqrt{2}c^2/ab)$ where a, b, and c are the cell parameters) and a value of 17.6° is obtained, in good agreement with other fluoroperovskites. The refined interatomic distances and bond angles of $NaFeF_3$ are shown in Table 1. From the atomic coordinates it is possible to directly estimate the polyhedral volume ratio,[26] which can be expressed as $V_A/V_B = (V_{cell}/4 - V_B)/V_B$ (V_A = volume of the NaF_{12} polyhedron, V_B = volume of the FeF_6 octahedra, and V_{cell} = volume of the unit cell) and

Table 1. Final Results of the Rietveld Refinements of Pv and pPv Forms of $NaFeF_3$ at Ambient Conditions Obtained from High-Resolution Data

perovskite		postperovskite	
a (Å)	5.66119(1)	a (Å)	3.13774(4)
b (Å)	7.88006(2)	b (Å)	10.20870(10)
c (Å)	5.48359(1)	c (Å)	7.45875(9)
V (Å^3)	244.626(1)	V (Å^3)	238.921(4)
space group	*Pnma*	space group	*Cmcm*
	Selected Bond Distances (Å)		
Fe−F1 × 2	2.0718(6)	Fe−F1 × 2	2.0529(11)
Fe−F2 × 2	2.0845(14)	Fe−F2 × 4	2.0831(12)
Fe−F2 × 2	2.0523(15)		
Na−F1	2.3091(26)	Na−F1 × 2	2.2795(20)
Na−F1	2.3397(25)		
Na−F2 × 2	2.3075(18)	Na−F2 × 4	2.4912(15)
Na−F2 × 2	2.6253(20)	Na−F2 × 2	2.5843(18)
Na−F2 × 2	2.7803(20)		
	Selected Bond Angles (deg)		
F1−Fe−F2	92.44(7)	F1−Fe−F1	85.48(6)
F1−Fe−F2	87.54(7)	F2−Fe−F2	97.72(8)
F2−Fe−F2^i	89.26(3)	Fe−F1−Fe	130.55(14)
Fe−F1−Fe	143.93(11)		
Fe−F2−Fe	144.58(8)		

takes the value of 4.2 in Pv $NaFeF_3$. Finally, the calculated bond valence sum (BVS) values of Na and Fe are consistent with the valence states Na^+ and Fe^{2+}.

The molar magnetic susceptibility χ_M measured as a function of temperature in an applied magnetic field H = 1 T on powder samples of Pv $NaFeF_3$ is presented in Figure 2. The data show a sharp increase of χ_M below 90 K, providing a clear signature of the onset of long-range magnetic ordering. At temperatures lower than 20 K, χ_M starts decreasing. It is well-known that $NaBF_3$ fluorides adopting the $GdFeO_3$ structure (B = Ni, Mn, Co) can be described as G-type antiferromagnets.[27−30] Weak ferromagnetism is observed below the Néel temperature T_N, which is associated with the presence of spin canting. Our data point toward a scenario where also $NaFeF_3$ can be described as a weak ferromagnet with T_N = 90 K in analogy with the other members of the family. As expected for this type of magnetic ordering, the temperature dependence of the ZFC and FC magnetization measured at the lower magnetic fields of 0.01 and 0.1 T show divergence below 90 K (Figure 2 and Supporting Information, Figure S1). Magnetization vs H curves were collected at different temperatures. At 4 K, a small hysteresis loop with coercive field of 2.4 mT is observed and the magnetization reaches the value of 0.36 μ_B/Fe atom at 9 T (Figure 2). The lack of Curie−Weiss behavior at temperatures well above T_N and the shape of the M vs H curve at 300 K demonstrate the absence of paramagnetic behavior, even at room temperature, and point toward the existence of an underlying magnetic contribution which could be due to the presence of impurities. Indeed, small traces (<0.5%) of unreacted α-Fe are visible in the high-resolution synchrotron diffraction profiles.

Perovskite $NaFeF_3$: Electronic Structure. To get further insight into the properties of the Pv phase of $NaFeF_3$, electronic structure calculations were performed. They were based on density functional theory at the GGA + U level to take into account the highly correlated nature of the Fe^{2+} d-electrons. Four different spin-ordered structures were considered as possible ground states: (i) F-type spin ordering with intra- and interlayer ferromagnetic arrangement; (ii) A-type spin ordering with intralayer ferromagnetic and interlayer antiferromagnetic spin arrangements; (iii) C-type spin ordering in which the magnetic centers interact antiferromagnetically with the in-plane nearest neighbors and ferromagnetically with those out of plane; (iv) G-type spin ordering with antiferromagnetic exchange with all the nearest neighbors (Supporting Information, Figure S4). The analysis of the exchange interactions was performed using the nearest-neighbor Heisenberg Hamiltonian which allows their evaluation from total energy calculations.[31,32] Two magnetic exchange parameters were considered to describe the interlayer (J_{ac}) and the intralayer (J_b) coupling in the orthorhombic Pv unit cell. The Hubbard parameter U was varied evenly in steps of 2 eV from 0.0 to 8.0 eV with the Hund's exchange parameter of J_H = 0.98 eV obtained from former local spin density approximation (LSDA) calculations on $KFeF_3$.[33] The calculated electronic energies of the different magnetic orderings are compared in Table 2. The magnetic ground state for $NaFeF_3$ corresponds to the G-type antiferromagnetic phase similar to analogous systems.[27−30] At U_{eff} > 7.02 eV the negative character of J_b becomes positive while J_{ac} remains negative. For calculations of the electronic density of states (DOS) and local density of states (LDOS) in the ground state G-type phase, the parameters U = 4 and J_H = 0.98 eV were used (Figure 3).

dx.doi.org/10.1021/ic502224y | *Inorg. Chem.* 2014, 53, 12205−12214

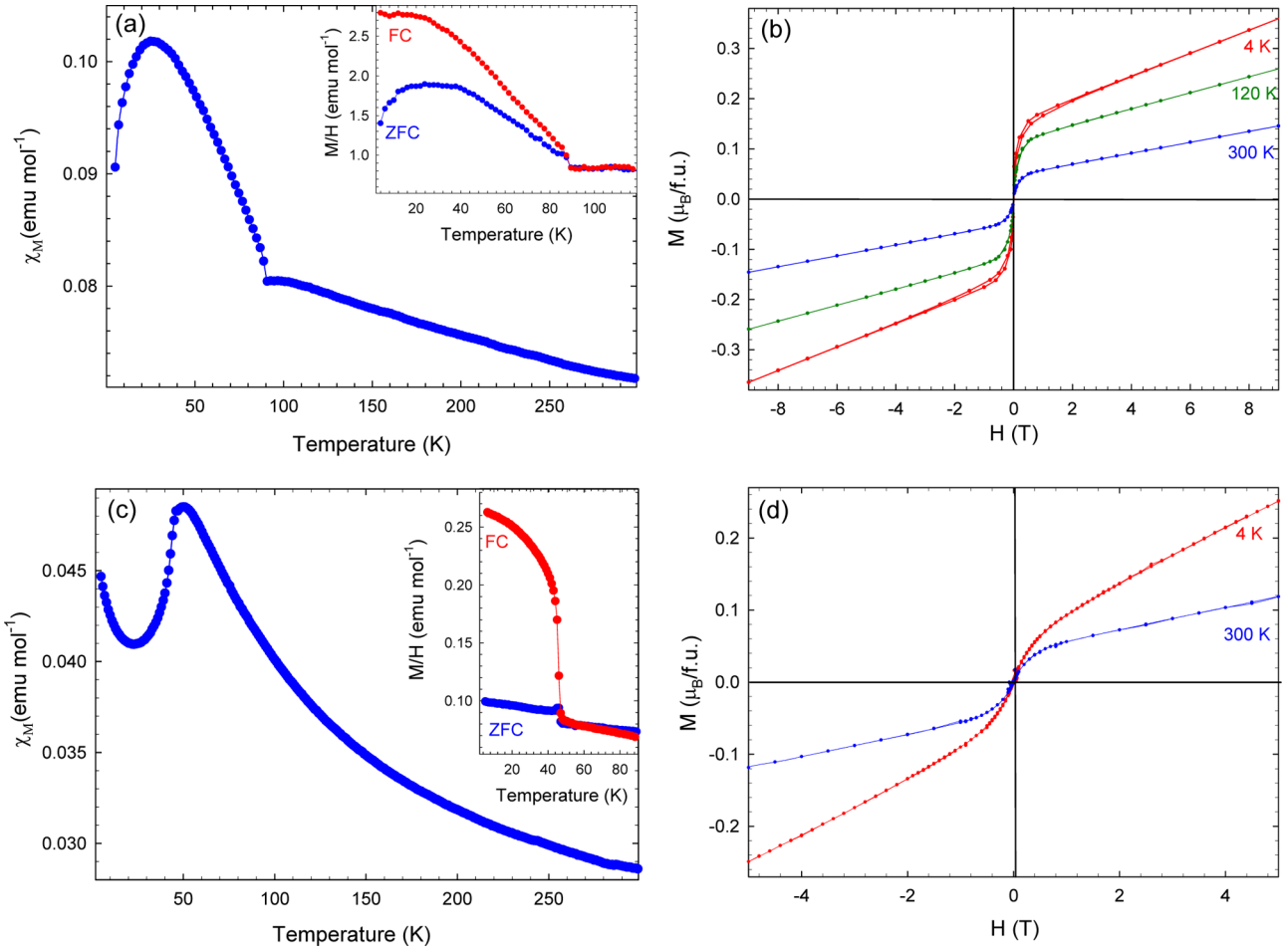

Figure 2. Temperature dependence of the magnetic susceptibility χ_M (H = 1 T) of (a) Pv and (c) pPv $NaFeF_3$. The insets of (a) and (c) show the ZFC/FC magnetization divided by the field (0.1 T) for Pv and pPv, respectively. Magnetic hysteresis loops (b) of Pv at 4, 120, and 300 K and (d) of pPv $NaFeF_3$ at 4 and 300 K.

Table 2. Relative Energies (in meV) of F-, A-, and C-Types with Respect to G-Type and the Interlayer (J_b) and Intralayer (J_{ac}) Exchange Parameters for Pv $NaFeF_3$ with Different Values of the Hubbard Parameter U

U	G (meV)	F (meV)	C (meV)	A (meV)	J_b (meV)	J_{ac} (meV)	E_g (eV)
0	0.0	43.8	15.1	27.6	−1.9	−1.7	0.49
2	0.0	43.6	13.2	29.7	−1.6	−1.8	1.33
4	0.0	27.7	8.1	19.0	−1.0	−1.2	2.59
6	0.0	13.5	3.3	12.0	−0.2	−0.6	3.52
8	0.0	67.7	2.1	11.5	0.1	−0.5	4.45

From the LDOS and DOS a d-orbital character can be observed at the periphery of the Fermi level, E_F. This result and the large band gap energy indicate that the $GdFeO_3$-type $NaFeF_3$ can be described as a Mott insulator. A high spin configuration (t_{2g}^4 e_g^2) is observed in LDOS. All five spin-up d-orbitals lie below the E_F, leaving one of the 3-fold degenerate t_{2g} orbitals to be occupied by electrons with a spin-down configuration according to Hund's rule. It can also be seen that only spin-down electrons do not forbid transfer to the lowest d-orbitals of the conduction band. The band gap E_g increases linearly as a function of the Hubbard term U: E_g = 0.47 eV at U = 0 and E_g = 4.56 eV at U = 8 eV. Recent nonmagnetic DFT calculations on $NaFeF_3$ with $U = U_{eff}$ and J = 4 eV resulted in E_g = 2.86 eV, supporting our results at U = 4.[34]

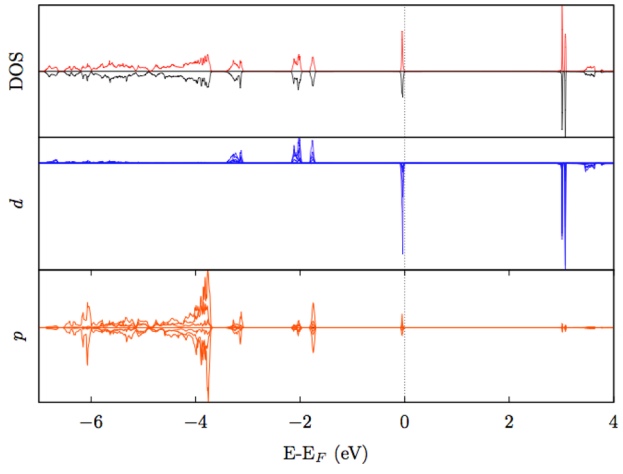

Figure 3. (top) DOS of Pv $NaFeF_3$, (middle) LDOS of d-orbitals of Fe^{2+} ions, and (bottom) LDOS of p-orbitals of F^- ions at U_{eff} = 3.02 eV in the G-type ground state magnetic ordering.

Perovskite to Postperovskite Transition. In order to observe a transition from Pv to a pPv-type structure, different criteria should be fulfilled. For instance, (i) the tolerance factor, t, should take a value between 0.8 and 0.9, (ii) the tilting angle,

dx.doi.org/10.1021/ic502224y | Inorg. Chem. 2014, 53, 12205−12214

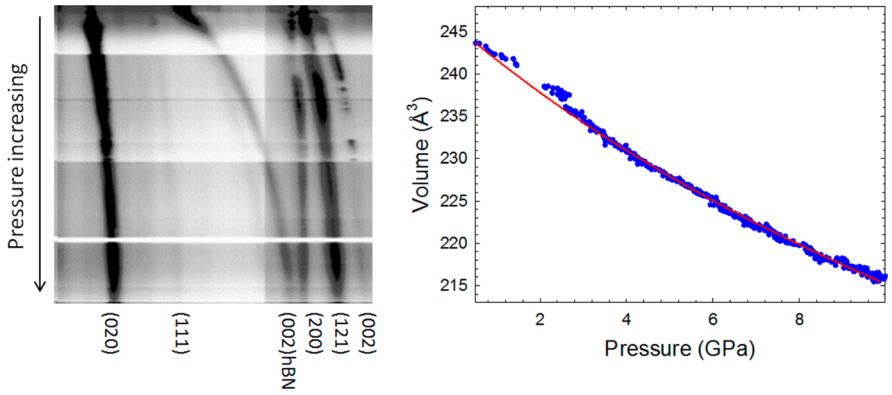

Figure 4. (left) Detail of in situ powder diffraction data showing behavior of principle reflections, taken at 298 K with increasing pressure (between ambient and 9 GPa) and (right) $p-V$ data obtained by sequential Rietveld refinements to these. The red curve is the third-order Birch−Murnaghan equation of state, with parameters fitted to these data.

ϕ, should be greater than about 13° at ambient conditions, and (iii) the polyhedral volume ratio V_A/V_B should take a value in the vicinity of 4.03.[35,36] As detailed in the section Perovskite NaFeF3: Crystal Structure and Magnetic Properties, $NaFeF_3$ fulfills all these prerequisites and its structural characteristics are very similar to those of other $GdFeO_3$-type fluoroperovskites ($NaBF_3$, B = Zn, Mg, Ni, Co) that undergo a transition to a pPv phase at high temperatures and pressures. For these reasons we attempted to observe such a transition in $NaFeF_3$ using the multianvil apparatus available on ID06 at the ESRF. A polycrystalline sample was first compressed to ∼10 GPa and then heated to approximately 1000 K. Powder diffraction profiles were collected at 32 s intervals over the 2.5 h compression at room temperature up to ∼9.7 GPa (Figure 4). The quality of the data allows automated refinement of cell parameters as a function of p, and thus enables the study of the behavior of different Pv structural parameters (e.g., axial/volume compressibilities and tilting angle). Inspection of the evolution of the diffraction profiles shows that, in the vicinity of 9 GPa, new peaks start appearing, clearly indicating the signature of a phase transformation. The $p-V$ data extracted up to this pressure for the Pv phase are plotted in Figure 4. The resulting values of the equation of state parameters with second- and third-order Birch−Murnaghan equations fitted to the $p-V$ data are K_0 = 55.2 (3) GPa and K_0 = 42.3(2) GPa and K' = 6.9(1), respectively (in both cases V_0 was fixed to 244.6 Å^3). The obtained values of K_0 imply that the Pv phase of $NaFeF_3$ is softer than related fluoroperovskites. In addition, the extracted axial compressibilities are quite large and anisotropic with β_c (7.1×10^{-3}) being 2.5 times as large as β_a (2.7×10^{-3}) (Supporting Information, Figure S3). This result is also reflected in the behavior of the tilting angle, which exhibits a dramatic response to increasing pressure and reaches the value of ϕ = 26° near the transition boundary. Following the increase in pressure to 9.7 GPa, the sample was then heated to ∼1000 K, again with continuous data acquisition. The diffraction profile collected at these conditions evidenced the coexistence of both Pv and pPv forms at all temperatures. However, the latter undergoes a retrograde transition to Pv at around 850 K. The lattice parameters of both polymorphs were extracted between ∼500 and 1000 K. The lattice constants of the Pv smoothly increase resulting in a volumetric expansion $\alpha_V = 1.41 \times 10^{-5}$ K^{-1}. This is accompanied by a decrease of ϕ, which reaches the value of 22.4° at 1000 K. A second run in the multianvil press was then performed to avoid the back transformation. A powder sample of Pv $NaFeF_3$ was then first compressed to 10 GPa and subsequently heated to 700 K. Diffraction profiles collected at these conditions confirmed the stabilization of a new phase that could not be identified as any other known compound in the Na−Fe−F phase diagram, implying the absence of phase decomposition or disproportionation. Standard indexing procedures quickly showed that all the Bragg reflections (excluding those relative to the cell assembly—BN and MgO) could be accounted for by considering a $CaIrO_3$-type orthorhombic lattice (space group *Cmcm*). Rietveld refinements confirmed the formation of the pPv phase with lattice constants a = 3.0180(1) Å, b = 9.6364(3) Å, and c = 7.2729(3) Å. The so-formed pPv phase was then quenched to room temperature while keeping the pressure at 10 GPa, and the obtained lattice constants at this condition are a = 3.0150(1) Å, b = 9.6134(2) Å, and c = 7.2217(2) Å (Figure 5). The assembly was then decompressed to ambient conditions.

High-resolution powder diffraction profiles were then collected on the recovered sample (Figure 6). Bragg peaks relative to the pPv are clearly visible together with reflections belonging to the Pv phase (24% phase fraction). It should be said that for this particular sample a small partial blowout of the capsule occurred during decompression, probably inducing back transformation of the metastable pPv to the more stable pV form. Subsequent multianvil runs performed at similar conditions produced pure samples of polycrystalline pPv $NaFeF_3$, thereby providing evidence that the phase is fully quenchable at ambient conditions. In addition, our recent single-crystal high pressure work has highlighted that the Pv to pPv phase transition can occur at RT in the absence of strain due to cold compression, but at pressures between 10 and 12 GPa. Also in that experiment, the pPv phase was found to be fully recoverable at atmospheric pressure.

The pPv Structure at Ambient Conditions. Rietveld refinements of the recovered pPv phase of $NaFeF_3$ at room temperature proceeded smoothly (Figure 6). The obtained values of the lattice constants are listed in Table 1 together with bond distances and angles. The resulting difference in volume between the Pv and the pPv is −2.3% ($\Delta V/V_0$). This value is consistent with those reported for other fluoroperovskites ABF_3 at ambient conditions. In the pPv structure the FeF_6 octahedra form "layers" which stack along the *b*-axis. They share edges along the *a*-axis and corners along the *c*-axis. The Fe−F1−Fe angle describes the degree of tilting of the octahedra along the *a*-axis and takes the value of 130.6°, which is smaller than that

dx.doi.org/10.1021/ic502224y | *Inorg. Chem.* 2014, 53, 12205−12214

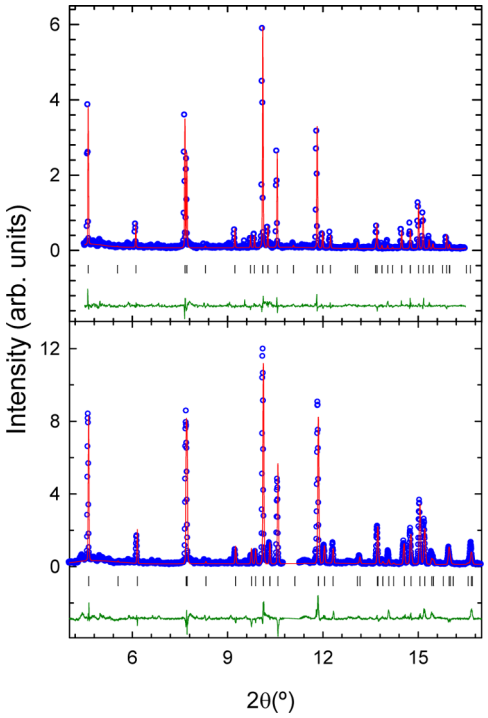

Figure 5. Final observed (○) and calculated (|) synchrotron powder X-ray diffraction profiles (λ = 0.3738 Å) for pPv $NaFeF_3$ at (top) 700 K and 10 GPa (a = 3.0180(1) Å, b = 9.6364(3) Å, and c = 7.2729(3) Å, space group *Cmcm*, agreement factors of the Rietveld refinement R_{wp} = 6.30%, R_{exp} = 4.83%) and (bottom) 298 K and 10 GPa (a = 3.0150(1) Å, b = 9.6134(2) Å, and c = 7.2218(2) Å, space group *Cmcm*, agreement factors R_{wp} = 6.05%, R_{exp} = 4.71%). The lower solid lines show the difference profiles, and the tick marks show the reflection positions.

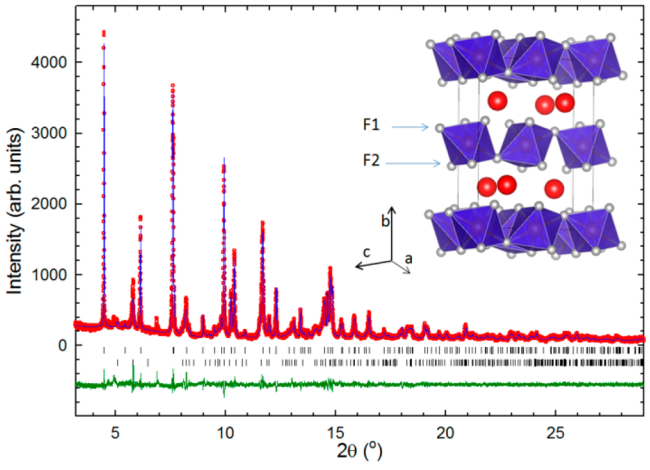

Figure 6. Final observed (○) and calculated (|) synchrotron powder X-ray diffraction profiles (λ = 0.3999 Å) for pPv $NaFeF_3$ at 298 K (a = 3.13774(1) Å, b = 10.2087(1) Å, and c = 7.45875(9) Å, space group *Cmcm*). Agreement factors of the Rietveld refinement: R_{wp} = 7.74; R_{exp} = 5.79%. The lower solid line is the difference profile, and the tick marks show the reflection positions. Pv $NaFeF_3$ is also present as a secondary phase (lower series of tick marks) with a weighted phase fraction of 24%. Low intensity peaks corresponding to spurious phases (e.g., BN) are also present.

of other fluoroperovskites, implying a higher degree of rugosity in the octahedral sheet. A comparison of important parameters that describe the octahedral distortion in the pPv phase for a number ABX_3 systems is shown in Table 3. In particular it is worth noticing that, at ambient conditions, the BF_6 octahedra of pPv $NaFeF_3$ are more distorted than in $NaNiF_3$. In addition, the polyhedral volume ratio, V_A/V_B, is significantly reduced from the ideal value of 5 (for a cubic structure) and approaches a value closer to that of $CaIrO_3$. BVS calculation performed on the refined structure showed that the Fe remains divalent in the pPv phase and no signature of a HS to LS transition is observed. It should be mentioned that the value of the bulk modulus of the pPv form obtained from single-crystal data on decompression is again lower compared to the analogous systems (K_0 = 48(2) GPa and K' = 7.2(4) obtained by fitting the data with a third-order Birch–Murnaghan equation).

On cooling from room temperature the pPv phase of $NaFeF_3$ is retained with a smooth decrease of the volume down to 10 K (Supporting Information, Figure S2). The lattice thermal expansivities calculated between 25 and 300 K are comparable for the crystallographic b (interlayer) direction and c-axis (Supporting Information, Figure S2). The a lattice constant, which is the edge-sharing direction, has a linear thermal expansivity that is 1 order of magnitude smaller. The FeF_6 octahedra are quite insensitive to cooling, but their distortion slightly decreases as exemplified by the bond-angle variance which takes the value of 28 at 10 K (cf. 36 at RT).

A single-phase sample of pPv $NaFeF_3$ was synthesized for magnetic characterization. χ_M measured as a function of temperature in an applied field of 1 T clearly shows (Figure 2) the presence of a cusp at low temperatures providing a strong indication of the onset of an antiferromagnetic transition at T_N = 48 K. As for the Pv phase, no Curie–Weiss behavior is observed at higher temperatures. In order to gain further insights on the nature of the magnetic transition, the spontaneous magnetization was measured at lower fields. Large differences are observed below T_N between the ZFC and FC protocols, suggesting spin canting (Figure 2 and Supporting Information, Figure S1). It appears that at low fields the pPv phase behaves as a weak ferromagnet, while increasing the field induces a spin realignment and a stronger antiferromagnetic response. The field dependence of the magnetization at 5 K also shows a small hysteresis loop confirming the presence of a small ferromagnetic component, but no signature of a spin-flop transition is evident. The magnetic behavior of pPv $NaFeF_3$ is somehow comparable to that observed in the analogous pPv phase of $NaNiF_3$ that can also be described as canted antiferromagnet (T_N = 22 K).[9] However, in this case, an increase in the applied field results in a larger ferromagnetic component.

Electronic and Magnetic Structures by DFT (pPv). Our magnetic measurements on pPv $NaFeF_3$ point toward a predominantly antiferromagnetic order. The magnetic exchange interactions are expected to be weaker in the pPv phase than in the parent Pv due to its layered structure. The nearly two-dimensional arrangement of the octahedra gives rise to a number of potential spin arrangements. Based on the unit cell of pPv $NaFeF_3$ four possible arrangements were considered: (i) A-type ordering corresponding to intralayer ferromagnetic and interlayer antiferromagnetic interactions; (ii) F-type phase with inter- and intralayer ferromagnetic interactions. Two further phases were considered with intralayer antiferromagnetic interactions: a ferromagnetic C′-type and an antiferromagnetic C″-type stacking as shown in the Supporting Information, Figure S5. The same setup parameters employed for Pv $NaFeF_3$ were used for the calculations on the pPv form. The collinear

dx.doi.org/10.1021/ic502224y | *Inorg. Chem.* 2014, 53, 12205–12214

Table 3. Selected Parameters of Pv and pPv $NaBF_3$ Fluoroperovskites[a]

	$NaFeF_3$	$NaNiF_3$	$NaCoF_3$	$NaZnF_3$	$NaMgF_3$	$MgSiO_3$
			Pv $NaBF_3$ Fluoroperovskites			
K_0[b] (GPa)	42.3	64	65	65	76	253
β_a[c] ($\times 10^{-3}$ GPa)	2.3	2.0	2.6	1.5		1.1
β_b[c] ($\times 10^{-3}$ GPa)	4.8	4.7	4.8	3.1		1.4
β_c[c] ($\times 10^{-3}$ GPa)	7.1	9	8.3	4.4		1.4
$V_{NaF_{12}}/V_{BF_6}$[d]	4.2	4.4	4.3	4.3	4.5	
t[e]	0.85	0.86	0.89	0.87	0.88	
ϕ[f]	17.6	17.2	17.7	17.3	15.0	
P_S[g] (GPa)	9	11−12	11−14	14−22	27−29	121
Ψ_S[h]	5.4	5.6	5.5	6.1	7.1	
$\Delta V/V_0$[i] (%)	−2.3	−1.7	−2.0	−1.9	−0.9	−1.5
			pPv $NaBF_3$ Fluoroperovskites			
B−X1	2.053	1.998		2.016	1.77	1.644
B−X2	2.083	2.008		2.034	1.83	1.664
X1−B−X2	94.6	92.3		92.6		91.2
X2−B−X2	82.3	82.2		83		84.9
B−X1−B	130.6	135.7		135.5		135.8

[a]The values relative to B = Ni, Co, Zn, and Mg as well as for $MgSiO_3$ are taken from ref 14. The bond distances and angles for the pPv phases refer to ambient conditions, while those for $MgSiO_3$ are calculated from data at 121 GPa and 300 K. [b]K_0: bulk modulus. [c]β_i: axial compressibility. [d]$V_{NaF_{12}}/V_{BF_6}$: polyhedral volume ratio. [e]t: tolerance factor. [f]ϕ: octahedral tilting angle at ambient conditions. [g]P_S: transition pressure at room temperature. [h]Ψ_S: stabilization factor (as defined in the text). [i]$\Delta V/V_0$: volume change at ambient conditions (for $MgSiO_3$, the high pressure value is shown).

magnetic ground state is degenerate between C′- and C″-type spin ordering at all levels of correlations in line with recent results on isostructural pPv $NaMnF_3$.[32] The spin interactions were first decoupled into interlayer (J_b) and intralayer (J_{ac}). The calculated interlayer antiferromagnetic interactions were lower than the numerical accuracy of ∼1 meV, and are not presented. The low accuracy predicted from the Heisenberg model implies feeble interlayer spin interactions and a quasi-two-dimensional magnetic structure. Strong intralayer J_{ac} spin interactions were otherwise found. Further decoupling of the J_{ac} parameter resulted in antiferromagnetic J_c and ferromagnetic J_a (Table 4).

Table 4. Relative Energies (in meV) of Various Hypothetical Magnetic Phases, Normalized to the Energy of the Ground State Which Has C′-Type Ordering[a]

U	C″ (meV)	A (meV)	C′ (meV)	F (meV)	J_c (meV)	J_a (meV)	E_g (eV)
0	0.0	18.9	0.0	19.2	−1.2	6667.7	0.38 (0.38)
2	0.0	15.6	0.0	15.8	−1.9	6605.8	1.18 (1.17)
4	0.0	9.3	0.0	9.5	−1.1	6505.2	2.69 (2.69)
6	0.0	5.3	0.0	5.5	−0.6	6426.7	3.66 (3.66)
8	0.0	2.8	0.5	2.8	−0.3	6369.3	4.62 (4.63)

[a]The exchange parameters (J_a) and (J_c) for pPv $NaFeF_3$ are also given with increasing level of the Hubbard term U. The band gap energy E_g was calculated using the degenerate ground state orderings C′ (in parentheses) and C″.

The strength of the ferromagnetic spin interactions along the *a*-axis is 3 orders of magnitude larger than the antiferromagnetic ones along the *c*-axis regardless the value of U. This can be explained from the rearrangement of the octahedra from three-dimensional vertex-sharing in Pv to corrugate laminar edge-sharing octahedra along the *a*-axis and vertex-sharing along the *c*-axis (compare Figure 1 and Figure 6). The edge-sharing geometry imposes Fe2−F−Fe2 angles close to 90°. This supports ferromagnetic interactions according to Good-enough−Kanamori rules, whereas antiferromagnetic ordering along the *c*-axis is expected (Fe−F1−Fe ∼ 130.6°). The fundamental electronic trends of the Pv phase are preserved after the transition (e.g., d-character around E_F and p-character at low energy values), suggesting that pPv $NaFeF_3$ can also be described as a Mott insulator. The band gap's dependency on the Hubbard parameter is analogous: E_g in C′-type ordering changes from 0.38 to 4.63 eV when U increases from 0 to 8 eV. The electronic structure of DOS and LDOS of Fe^{2+} at U = 4 of the collinear C′-type phase is presented in Figure 7. The high-

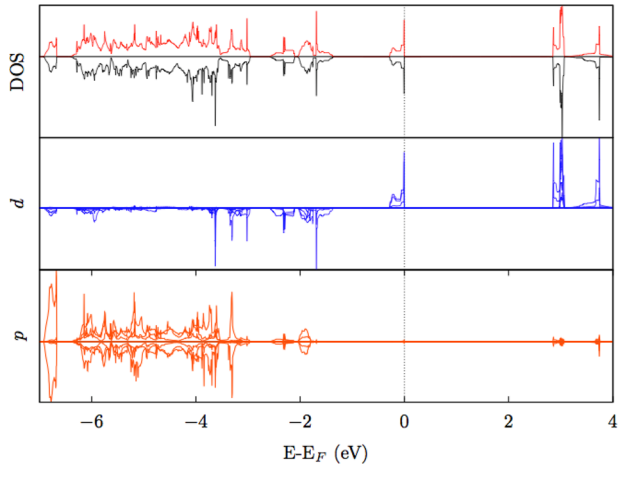

Figure 7. (top) DOS of pPv $NaFeF_3$, (middle) LDOS of d-orbitals of Fe^{2+} ions, and (bottom) LDOS of p-orbitals of F^- ions at U_{eff} = 3.02 eV in the C′-type ground state magnetic ordering.

spin configuration is also preserved after the structural phase transition. However, the new octahedral arrangement displays only two types of bonds (large basal bonds (2.1138 Å) and short (2.054 Å) axial bonds) reflected on the orbital occupancy in LDOS.

dx.doi.org/10.1021/ic502224y | Inorg. Chem. 2014, 53, 12205−12214

DISCUSSION

The experimental structural and magnetic characterizations coupled with theoretical calculations show that the original Pv phase of $NaFeF_3$ can be described as a Mott−Hubbard insulator which undergoes an antiferromagnetic transition below 90 K. The DFT calculations indicate a G-type magnetic structure as ground state, well in line with previous experimental and theoretical studies on analogous systems. The crystal structure of the Pv phase at ambient conditions is directly comparable to other $NaBF_3$ systems with only slightly more distorted FeF_6 octahedra. Increasing pressure at room temperature induces the transition to pPv, which starts at 9 GPa in powder samples. It is known that other fluoroperovskites with B = Co, Ni, and Zn show an analogous behavior and the pPv phase starts forming at pressures between 11 and 14 GPa at ambient temperature.[8,9,13] The low stabilization pressure of pPv $NaBF_3$ could be linked to the values of the axial compressibilities, which are very strongly anisotropic and result in a more rapid increase of the tilting angle with p. As pointed out by Tsuchiya et al., the mechanism for the Pv to pPv transition in ABO_3 $GdFeO_3$-type oxides involves tilting of relatively rigid BO_6 octahedra.[37] It has been demonstrated that the Pv−pPv transformation would only take place if the value of ϕ for the Pv phase lies between 13 and 15° at ambient conditions, and increases with pressure. If ϕ is less than 13°, then it would decrease with pressure and the Pv to pPv transition would be precluded. This approach is nonetheless impeded by the assumption that the octahedra are undistorted in the original Pv orthorhombic phase (which is strictly not exact). Yet, Tateno et al. have shown that it holds well for the oxides and the transition to pPv takes place when ϕ reaches a value of 26−27°.[36] Yusa et al. extended the relationship between ϕ and transition pressure to the fluoroperovskites and demonstrated its validity.[8] Indeed, our results are in line with these observations, and in the case of $NaFeF_3$, ϕ, which assumes a value of 17.6° at ambient conditions in the original Pv phase, reaches the critical value of 26° at pressures below those for analogous systems (Figure 8).

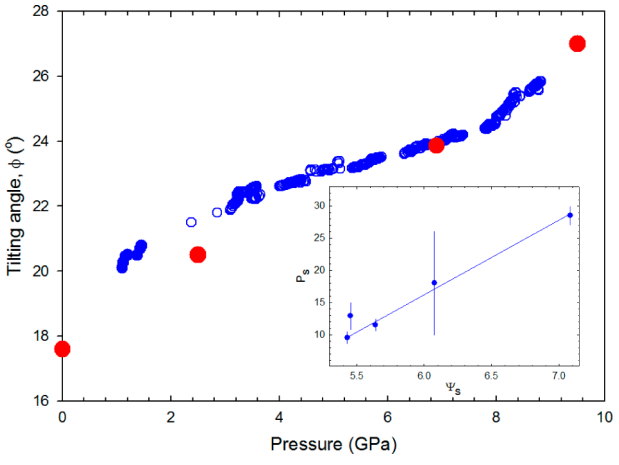

Figure 8. Pressure evolution of the octahedral tilting angle of Pv $NaFeF_3$. The blue circles correspond to the large-volume-press (LVP) data collected between ambient and 9 GPa. The values obtained from the single crystal DAC experiment (red circles) are also added for comparison (taken from ref 17). Inset: plot of room temperature pPv stabilization pressures against the stabilization factor for various $NaBF_3$ systems (see Table 3 for details).

The extreme sensitivity of the tilting angle to pressure can also be directly linked to the difference in compressibilities between the Fe−F and the Na−F bonds. The volume reduction upon increasing pressure is achieved by increasing the tilts of the FeF_6 octahedra, but critically, this is only possible if the Fe−F bonds are less compressible than the Na−F bonds. Zhao et al. have developed an elegant method to predict the ratio of the cation polyhedral compressibilities β_B/β_A in terms of a parameter M which represents the variation in the bond valence sum at the cation site due to the change of the average bond distance.[38] The ratio of β_B/β_A is then given in terms of the ratio of the calculated M values for the AF_{12} (or AF_8) and BF_6 polyhedra according to the relationship

$$\frac{b_B}{b_A} = \frac{M_A}{M_B} = \frac{R_i N_i}{B} \exp\left[\frac{R_o - R_i}{B}\right]$$

where R_i is the average bond distance, N_i is the coordination number, and R_o and B are the bond valence parameters. In the case of $NaFeF_3$ M_A/M_B = 0.37 considering a NaF_{12} dodecahedral site (M_A/M_B = 0.53 for NaF_8), implying that the compressibility of the NaF_{12} polyhedron is substantially larger than that of FeF_6 octahedron. The same calculation performed on B = Ni, Co, and Mg shows that the equivalent values are 0.44, 0.42, and 0.46 respectively. As most of the variation in the M_A/M_B ratio is due to the different values of M_A for the Na site, we can assume that a larger ratio implies a less compressible NaF_{12} polyhedron. Therefore, higher pressures are needed to reach the critical value of the tilting angle for the transition to a postperovskite to occur. The values of the M_A/M_B ratio could also be correlated to the measured bulk modulus as the AF_{12} sites are more compressible and then contribute more to the total volume response. Given the paucity of reliable published crystal structures for different $GdFeO_3$ fluoroperovskites, it is difficult to draw relationships between M_A/M_B and bulk modulus as it has been established, for instance, for A = Ca in ABO_3 $GdFeO_3$-type oxides.[39] However, we note that also in the ABF_3 systems, higher values of M_A/M_B correspond to larger values of the bulk moduli with $NaFeF_3$ displaying the smallest values of both quantities.

Many authors have discussed the factors that are important for ABX_3 $GdFeO_3$-type perovskites to undergo the transition to pPv phases at ambient or high pressures. These are (i) the relative sizes of the cations and anion (ionic radii) which can be expressed, for instance, in terms of the tolerance factor, and (ii) the degree of covalency of the B−X bond. It has been found that systems where the difference in electronegativity between the B cation and the X anion is large (the bond is more ionic) will tend to transform to pPv at higher pressures. This can be understood considering that a more covalent B−X bond will reduce the anion−anion repulsion and therefore favor the edge-sharing geometry of the octahedral in the pPv structure. Akaogi et al. have examined this point in great detail for both ABX_3 fluoride and oxides.[14] An interesting approach is the one developed by Lindsay-Scott,[40] who combined the two factors listed above and defined a new parameter, the stabilization factor, Ψ_S, which is expressed as

$$\Psi_S = \frac{r_B + r_X}{r_B} \Delta\chi_{i(X-B)}$$

where r_B and r_X are the ionic radii of the B cation and the X anion, respectively, while $\Delta\chi_{i(X-B)}$ is the difference in Pauling electronegativity between the two. A linear relationship was

dx.doi.org/10.1021/ic502224y | Inorg. Chem. 2014, 53, 12205−12214

found between Ψ_S and the stabilization pressure (at ambient temperature) of various ABO_3 pPv phases. In an attempt to understand if the ABF_3 fluoroperovskites also follow an analogous trend, we have calculated Ψ_S and plotted it against the experimental room temperature pPv stabilization pressures, P_S (taken as the pressure at which Bragg peaks relative to pPv phase are observed on polycrystalline samples). Despite the obvious uncertainties on the exact transition pressure and the limited data available, it appears that a linear relationship can be established also for the fluoroperovskites (Figure 8 and Table 3). Such a relationship can be used to estimate the P_S values of other $GdFeO_3$-type fluorides yet to be studied. For instance, if the linear relationship holds, $NaMnF_3$ should transform into the pPv at ∼16 GPa. Unfortunately, this system is reported to undergo phase decomposition at high temperatures and pressures and no pPv phase has yet been isolated. A recent theoretical work places the Pv to pPv transition in $NaMnF_3$ at 8 GPa which was evaluated considering only the computed evolution of the tilting angle as a function of p. Among other fluorides, $KAgF_3$ (t = 0.82, ϕ = 15.6) would be a good candidate to test as its values of Ψ_S will place the transition below 4 GPa at room temperature.

Our data do not allow the determination of the Clapyeron slope of the Pv to pPv transition boundary, and more experiments are needed for its evaluation. The $NaBF_6$ studied so far (B = Ni, Co, Zn) show a positive value of dp/dT in the range between 10 and 16 MPa/°C (cf. $MgSiO_3$, 13.3 MPa/°C). We recall that, in the Pv phase of $NaFeF_3$, ϕ depends on temperature and a substantial decrease is observed upon heating from RT to 1000 K. This implies that at high temperature the value of ϕ will tend to become smaller and move further away from the critical value that is needed for the transformation to occur. This is consistent with a positive value of the Clapyeron slope for the transition boundary as higher temperatures stabilize the Pv phase over the pPv.

The discussion above shows that there are a number of analogies in the crystal-chemical characteristics of the Pv to pPv transition in $GdFeO_3$-type oxides and fluorides. Many of the factors that govern the formation and stabilization of the $CaIrO_3$ type are common (e.g., trends in tilting angle and stabilization pressure). In addition, also the structural parameters of pPv $NaBF_3$ are directly comparable to those of $MgSiO_3$ pPv at high p and T. For instance, the values of the bond distances and angles in pPv $NaBF_3$ describe a structure where the distortion of the BF_6 octahedra is generally small and the edge-sharing geometry is quite regular. The prototype $CaIrO_3$ shows an important distortion of the octahedra due to the Jahn−Teller distortions, and the structural parameters are substantially different from those of pPv $MgSiO_3$ (this is also true for the related $CaRuO_3$ and $CaRhO_3$) implying that the behavior of the two systems upon increasing p and T may not be directly comparable. Among the fluorides, no striking differences are observed in the values of bond lengths and angles of the two fully quenchable pPv phases $NaFeF_3$ and $NaNiF_3$, and as such both of them can be considered suitable low-pressure analogues of pPv $MgSiO_3$. Comparing the structural parameters of the two systems, it seems that the BF_6 octahedra are more distorted in $NaFeF_3$ and the octahedral sheets are less planar. However, given that in $NaFeF_3$ the transition occurs at lower pressures, that makes the study of this particular system very attractive, not only to get further insights into the implications of the transition but also to search for higher density phases above pPv.

Particularly interesting is the magnetic behavior of the pPv phase of $NaFeF_3$. Upon the pV to pPv transition Fe^{2+} maintains its high spin state. DFT calculations point toward a quasi-two-dimensional magnetic structure with competing antiferromagnetic and ferromagnetic interactions. The magnetic measurements are in line with this description, showing the signature of a typical canted antiferromagnetic transition with the degree of canting being quite sensitive to the applied magnetic field. Neutron diffraction measurements are in progress to get further insights into the magnetic structure of pPv $NaFeF_3$.

CONCLUSION

The most prominent point arising from our results is that $GdFeO_3$-type $NaFeF_3$ can be added to the family of ternary fluoroperovskites that transform to a pPv phase. The transition starts occurring at pressures as low as 9 GPa at room temperature in polycrystalline samples. The substantially larger compressibility of the AF_{12} sites over the NaF_6 octahedra results in the tilting angle increasing upon compression, reaching quite rapidly the critical value for the transition to occur. The pPv phase is fully quenchable down to ambient conditions. The crystal-chemical characteristics of the pV−pPv transition are quite similar to those reported for other members of the fluoroperovskite family and for the ABO_3 oxides. Both pV and pPv forms of $NaFeF_3$ can be described as Mott insulators and behave as canted antiferromagnets at low temperatures.

ASSOCIATED CONTENT

Supporting Information

Crystallographic data in CIF format. Room temperature refined atomic coordinates of Pv and pPv phases of $NaFeF_3$, ZFC/FC magnetization divided by the field (0.01 T) for both forms, temperature evolution of the normalized lattice constants and unit cell volume of pPv $NaFeF_3$ between 10 and 300 K, pressure evolution of the normalized lattice constants of Pv $NaFeF_3$, different collinear magnetic structures used in the DFT calculations for both forms. This material is available free of charge via the Internet at http://pubs.acs.org.

AUTHOR INFORMATION

Corresponding Author

*E-mail: serena.margadonna@kjemi.uio.no.

Notes

The authors declare no competing financial interest.

ACKNOWLEDGMENTS

The ESRF is thanked for allocation of beamtime at ID06LVP and ID31 (now ID22). The studentship of F.L.B. is supported by NFR Project 214260 of the Norges forskningsråd to S.M.

REFERENCES

(1) Tressaud, A.; Dance, J. M. *Struct. Bonding (Berlin)* **1982**, *52*, 89−146.
(2) Scatturin, V.; Corliss, L.; Elliott, N.; Hastings, J. *Acta Crystallogr.* **1961**, *14*, 19−26.
(3) Binggeli, N.; Altarelli, M. *Phys. Rev. B* **2004**, *70*, 085117.
(4) Margadonna, S.; Karotsis, G. *J. Am. Chem. Soc.* **2006**, *128*, 16436−16437.
(5) Yamauchi, K.; Picozzi, S. *Phys. Rev. Lett.* **2010**, *105*, 10720.
(6) Dobson, D. P.; Hunt, S. A.; Lindsay-Scott, A.; Wood, I. G. *Phys. Earth Planet. Inter.* **2011**, *189*, 171−175.

(7) Martin, C. D.; Crichton, W. A.; Liu, H. Z.; Prakapenka, V.; Chen, J. H.; Parise, J. B. *Am. Mineral.* **2006**, *91*, 1703−1706.
(8) Yusa, H.; Shirako, Y.; Akaogi, M.; Kojitani, H.; Hirao, N.; Oishi, Y.; Kikegawa, T. *Inorg. Chem.* **2012**, *51*, 6559−6566.
(9) Shirako, Y.; Shi, Y. G.; Aimi, A.; Mori, D.; Kojitani, H.; Yamaura, K.; Inaguma, Y.; Akaogi, M. *J. Solid State Chem.* **2012**, *191*, 167−174.
(10) Oganov, A. R.; Ono, S. *Nature* **2004**, *430*, 445−448.
(11) Tsuchiya, T.; Tsuchiya, J.; Umemoto, K.; Wentzcovitch, R. M. *Earth Planet. Sci. Lett.* **2004**, *224*, 241−248.
(12) Dobson, D. P.; Miyajima, N.; Nestola, F.; Alvaro, M.; Casati, N.; Liebske, C.; Wood, I. G.; Walker, A. M. *Nat. Geosci.* **2013**, *6*, 575−578.
(13) Yakovlev, S.; Avdeev, M.; Mezouar, M. *J. Solid State Chem.* **2009**, *182*, 1545−1549.
(14) Akaogi, M.; Shirako, Y.; Kojitani, H.; Nagakari, T.; Yusa, H.; Yamaura, K. *Phys. Earth Planet. Inter.* **2014**, *228*, 160−169.
(15) Martin, C. D.; Crichton, W. A.; Liu, H. Z.; Prakapenka, V.; Chen, J. H.; Parise, J. B. *Geophys. Res. Lett.* **2006**, *33*, L11305.
(16) Benner, G.; Hoppe, R. *J. Fluorine Chem.* **1990**, *46*, 283−295.
(17) Crichton, W. A.; Bernal, F. L. M.; Guignard, J.; Hanfland, M.; Margadonna, S. 2014, arXiv:1410.2783 [cond-mat.mtrl-sci]. arXiv.org e-Print archive. http://arxiv.org/abs/1410.2783 (accessed Oct 10, 2014).
(18) Umemoto, K.; Wentzcovitch, R. M. *Proc. Natl. Acad. Sci. U.S.A.* **2008**, *105*, 6526−6530.
(19) Umemoto, K.; Wentzcovitch, R. M. *Phys. Rev. B* **2006**, *74*, 224105.
(20) Umemoto, K.; Wentzcovitch, R. M.; Allen, P. B. *Science* **2006**, *311*, 983−986.
(21) Larson, A. C.; Von Dreele, R. B. *General Structure Analysis System (GSAS)*; Los Alamos National Laboratory Report LAUR 86-748; Los Alamos National Laboratory: Los Alamos, NM, 2000.
(22) Toby, B. H. *J. Appl. Crystallogr.* **2001**, *34*, 210−213.
(23) Kresse, G.; Hafner, J. *Phys. Rev. B* **1993**, *47*, 558−561.
(24) Kresse, G.; Furthmuller, J. *Phys. Rev. B* **1996**, *54*, 11169−11186.
(25) Perdew, J. P.; Burke, K.; Ernzerhof, M. *Phys. Rev. Lett.* **1996**, *77*, 3865−3868.
(26) Kubo, A.; Kiefer, B.; Shim, S.; Shen, G.; Prakapenka, V. B.; Duffy, T. S. *Am. Mineral.* **2008**, *93*, 965−976.
(27) Shane, J. R.; Lyons, D. H.; Kestigan, M. *J. Appl. Phys.* **1967**, *38*, 1280−1282.
(28) Friedman, Z.; Melamud, M.; Makovsky, J.; Shaked, H. *Phys. Rev. B* **1970**, *2*, 179−181.
(29) Garcia-Castro, A. C.; Spaldin, N. A.; Romero, A. H.; Bousquet, E. *Phys. Rev. B* **2014**, *89*, 104107.
(30) Garcia-Castro, A. C.; Romero, A. H.; Bousquet, E. *Phys. Rev. B* **2014**, *90*, 064113.
(31) Rivero, P.; Moreira, I. P. R.; Illas, F. *J. Phys.: Conf. Ser.* **2008**, *117*, 012050.
(32) Wang, G.; Li, Z.; Zheng, L.; Yang, Z. *Phys. Rev. B* **2011**, *84*, 045111.
(33) Punkinnen, M. *Solid State Commun.* **1999**, *111*, 477−481.
(34) Yu, S.; Zhang, P.; Li, A.; Zhu, Z.; Yang, Y. *J. Solid State Electrochem.* **2014**, *18*, 2071−2075.
(35) Martin, C. D.; Parise, J. B. *Earth Planet. Sci. Lett.* **2008**, *265*, 630−640.
(36) Tateno, S.; Hirose, K.; Sata, N.; Ohishi, Y. *Phys. Earth Planet. Inter.* **2010**, *181*, 54−59.
(37) Tsuchiya, T.; Tsuchiya, J.; Umemoto, K.; Wentzcovitch, R. M. *Earth Planet. Sci. Lett.* **2004**, *224*, 241−248.
(38) Zhao, J.; Ross, N. L.; Angel, R. J. *Acta Crystallogr., B* **2006**, *62*, 431−439.
(39) Zhao, J.; Ross, N. L.; Angel, R. J. *Acta Crystallogr., B* **2004**, *60*, 263−271.
(40) Lindsay-Scott, A. *The Thermoelastic Properties of Post-Perovskite Analogue Phases*. Ph.D. Thesis, Department of Earth Sciences, University College London, 2011.